Chen, Chun-Wei; Lera, Natalia; Chaunsali, Rajesh; Torrent, Daniel; Álvarez, José Vicente; Yang, Jinkyu; San-José, Pablo; Christensen, Johan (2019). Mechanical analogue of a Majorana bound state. *Advanced Materials*, 31(51), 1904386, p.: 1-6.

DOI: https://doi.org/10.1002/adma.201904386

Mechanical analogue of a Majorana bound state

Chun-Wei Chen,[1,*] Natalia Lera,[2,*] Rajesh Chaunsali,[1] Daniel Torrent,[3] Jose Vicente Alvarez,[2] Jinkyu Yang,[1,†] Pablo San-Jose,[4,‡] and Johan Christensen[5,§]

[1] *Aeronautics and Astronautics, University of Washington, Seattle, WA 98195-2400, USA*

[2] *Departamento de Física de la Materia Condensada, Universidad Autónoma de Madrid, Madrid 28049, Spain, Condensed Matter Physics Center (IFIMAC) and Instituto Nicolás Cabrera*

[3] *GROC, UJI, Institut de Noves Tecnologies de la Imatge (INIT), Universitat Jaume I, 12071, Castelló, Spain*

[4] *Materials Science Factory, Instituto de Ciencia de Materiales de Madrid (ICMM-CSIC), Sor Juana Inés de la Cruz 3, 28049 Madrid, Spain*

[5] *Department of Physics, Universidad Carlos III de Madrid, ES-28916 Leganès, Madrid, Spain*

[*] These authors contributed equally

[†] Corresponding author.

jkyang@aa.washington.edu

[‡] Corresponding author.

pablo.sanjose@csic.es

[§] Corresponding author.

johan.christensen@uc3m.es

The discovery of topologically non-trivial electronic systems has opened a new age in condensed matter research. From topological insulators to topological superconductors and Weyl semimetals, it is now understood that some of the most remarkable and robust phases in electronic systems (e.g., Quantum Hall or Anomalous Quantum Hall) are the result of topological protection. These powerful ideas have recently begun to be explored also in bosonic systems. Topologically protected *acoustic*, *mechanical* and *optical* edge states have been demonstrated in a number of systems that recreate the requisite topological conditions [1–9]. Such states that propagate without backscattering could find important applications in communications and energy technologies. In this work we demonstrate a topologically *bound* mechanical state, a different class of non-propagating protected state that cannot be destroyed by local perturbations. It is in particular a mechanical analogue of the well known Majorana bound states of electronic topological superconductor systems [10, 11]. We implement the topological binding by creating a Kekulé distortion vortex [12] on a two-dimensional mechanical honeycomb superlattice which can be mapped to a magnetic flux vortex in a topological superconductor.

Topologically protected states emerge at topological defects of a gapped band structure. This general statement takes its simplest form in topological insulators [13], electronic systems with a gap at the Fermi level that is topologically distinct from that of vacuum or conventional insulators. At the boundary between a topological insulator and vacuum, the topological index is forced to change and thus, the boundary is a topological defect from the electronic point of view. It develops protected edge states that are robust against perturbations. These topological states are a manifestation of bulk topology, and their emergence is sometimes dubbed the bulk-boundary correspondence principle. This same principle has been exploited in the field of topological mechanics, which recently emerged as a fertile ground to explore bosonic analogues of protected electronic states, both in terms of static deformations in Maxwell lattices [14] and of elastic wave motions. As an example of the latter, artificial gyroscopic lattices have been shown to sustain robust chiral edge states by mimicking the quantum Hall effect [5, 15]. Other phononic metamaterials have been constructed to enable mechanical versions of the quantum spin Hall effect [6–8] and the valley degree of freedom [16] for unidirectional phononic signal guiding.

Topological modes at an extended boundary are propagating, but this is not generic. Prominent examples of bound states have been reported in Maxwell lattices for static floppy modes [14, 17], 1D spring-connected dimer chains [18] and photonic Majorana zero-mode crystals [19, 20]. Other notable examples of 0D states emerge in higher-order topological insulators that are characterized by a quantized nontrivial bulk polarization [21–23]. In electronics, a paradigmatic type of topological bound state is formed at point-like boundaries between two topologically-distinct one-dimensional (1D) superconductors [24]. Such states have unique properties (zero energy, charge and spin) and are known as Majorana bound state (MBS), due to their peculiar self-conjugate $\gamma = \gamma^\dagger$ nature (half-electron, half-hole). They were invented by Ettore Majorana in 1937 in a rather different context [25]. Implementations of MBSs were first proposed in quantum field theory by Jackiw and Rossi [26]. Condensed matter realisations were proposed by Read and Green in 2000 within the Quantum Hall phase [27], by Kitaev in 2001 in p-wave superconductors [10], and others [11, 28–30], with several recent experimental confirmations [31–34]. MBSs have been studied as possible building blocks of fault-tolerant quantum computers [35], and are the subject of intense research currently [36–38].

The original proposal by Jackiw and Rossi [26] is based on a two-dimensional Dirac system. They showed that the addition of a gap-opening pairing $\Delta(\boldsymbol{r})$ in the form of a vortex, a topological, zero-energy Majorana state becomes trapped at the vortex core. It was later shown that this proposal for the Dirac equation can be mapped onto magnetic flux vortices in spinless, p-wave superconductors [39, 40], thus connecting it to alternative condensed matter realisations of MBSs. In both realizations, the bound state retains its Majorana self-conjugate character, as it is always an equal superposition of the two fields coupled by the gap-opening Δ, be it charge-conjugate ultrarelativistic Dirac fermions or particle and holes in the superconductor (see Supporting Information for details).

In this work we demonstrate a mechanical mode topologically bound to a vortex, created by distorting a lattice of bolts attached on a thin aluminum plate free to vibrate. The binding mechanism is a mechanical version of the one in the Jackiw-Rossi model. The resulting bound state is an analogue of the Jackiw-Rossi MBS, wherein the two charge-conjugate $(+/-)$ Dirac fermions $\psi_{+/-,\uparrow/\downarrow}$ of the latter for different spin $(\uparrow / \downarrow)$ are exactly mapped into internal valley (K/K') degrees of freedom of the mechanical waves $c_{K/K',A/B}$

FIG. 1. **Kekulé distorted mechanical graphene**. A honeycomb lattice of bolts is attached to an oscillating plate. Shifting the position of bolts following a Kekulé pattern gaps the modes. The Kekulé gap has an internal phase $\phi(\boldsymbol{r})$ in valley space that can create a vortex (see gapped Dirac cones and phase arrows around the perimeter). A Kekulé vortex traps a topologically protected mode (in black and yellow), a mechanical analogue of a Majorana bound state.

in two sublattices (A/B), see Supporting Information for additional details of the mapping,

$$\psi_{+,\uparrow/\downarrow} = c_{K,A/B} \tag{1}$$
$$\psi_{-,\uparrow/\downarrow} = c_{K',B/A}.$$

The valley and sublattice degrees of freedom arise from the structure of the lattice, fabricated by attaching steel bolts on the plate in a honeycomb pattern. This give rise to Dirac-like flexural modes, i.e. a kind of *mechanical graphene* [7, 41, 42]. The vortex is then realised by deforming the honeycomb pattern following a Kekulé distortion. The resulting pattern of bolts, honeycomb plus distortion, is rendered in Fig. 1. The former produces a spectrum of plate modes analogous to graphene's, with two valleys around wavevectors $\boldsymbol{K}$ and $\boldsymbol{K}' = -\boldsymbol{K}$ and a Dirac-like dispersion around a specific Dirac frequency Ω_D in each of them. The Kekulé distortion field takes the form of an in-plane displacement $\delta\boldsymbol{r}(\boldsymbol{r})$ in the bolt positions,

$$\delta\boldsymbol{r}(\boldsymbol{r}) = d(r)\left[\sin(\boldsymbol{K}\boldsymbol{r} + \phi(\boldsymbol{r})), \pm\cos(\boldsymbol{K}\boldsymbol{r} + \phi(\boldsymbol{r}))\right], \tag{2}$$

where $\boldsymbol{K} = [4\pi/3a, 0]$ is the valley wavevector, a is the honeycomb period, and $\pm$ correspond to the two sublattices. This distortion is designed to induce a complex-valued intervalley coupling $\Delta = |\Delta|e^{i\phi}$ on the plate vibrations, with modulus $\sim d(\boldsymbol{r})/a$ and phase $\phi(\boldsymbol{r})$, see Supplementary Information. The precise shape of the radial profile $d(\boldsymbol{r})$ is unimportant with regards to topologial binding. Here we choose $d(r) = d_0 \tanh(r/\xi)$, a common model for superconducting vortices [43], with $d_0 = 0.15a$ and vortex radius $\xi = 0.1a$. The only crucial property of $\delta\boldsymbol{r}(\boldsymbol{r})$ and the induced $\Delta(\boldsymbol{r})$ is that the phase $\phi(\boldsymbol{r})$ creates a vortex with finite vorticity n, as in $\phi(\boldsymbol{r}) = n\phi_{\boldsymbol{r}}$, where $\phi_{\boldsymbol{r}}$ is the polar coordinate around the origin, $\boldsymbol{r} = r(\cos\phi_{\boldsymbol{r}}, \sin\phi_{\boldsymbol{r}})$. We concentrate on a vortex of minimal vorticity $n = 1$.

To understand the gap-opening effect of the distortion, consider a spatially uniform $d(\boldsymbol{r}) = d_0$ and ϕ. The honeycomb lattice remains periodic (see Fig. 2a), but the distortion triples the size of the unit cell, which folds the two Dirac cones onto the Γ-point and opens a gap $\sim d_0/a$. The gap changes slightly as a function of the phase ϕ, but never closes. The vortex lattice, in contrast, is no longer periodic (see Fig. 2b). The phase $\phi(\boldsymbol{r})$ does a full turn as $\boldsymbol{r}$ moves around the vortex core, but since d_0 remains finite the local gap around the periphery never closes (see Fig. 1 and supplementary video.)

The Jackiw-Rossi theory predicts that such a Kekulé 2D vortex binds a Majorana-like mode at its core at the Dirac point frequency, which in our concrete example of a bolted

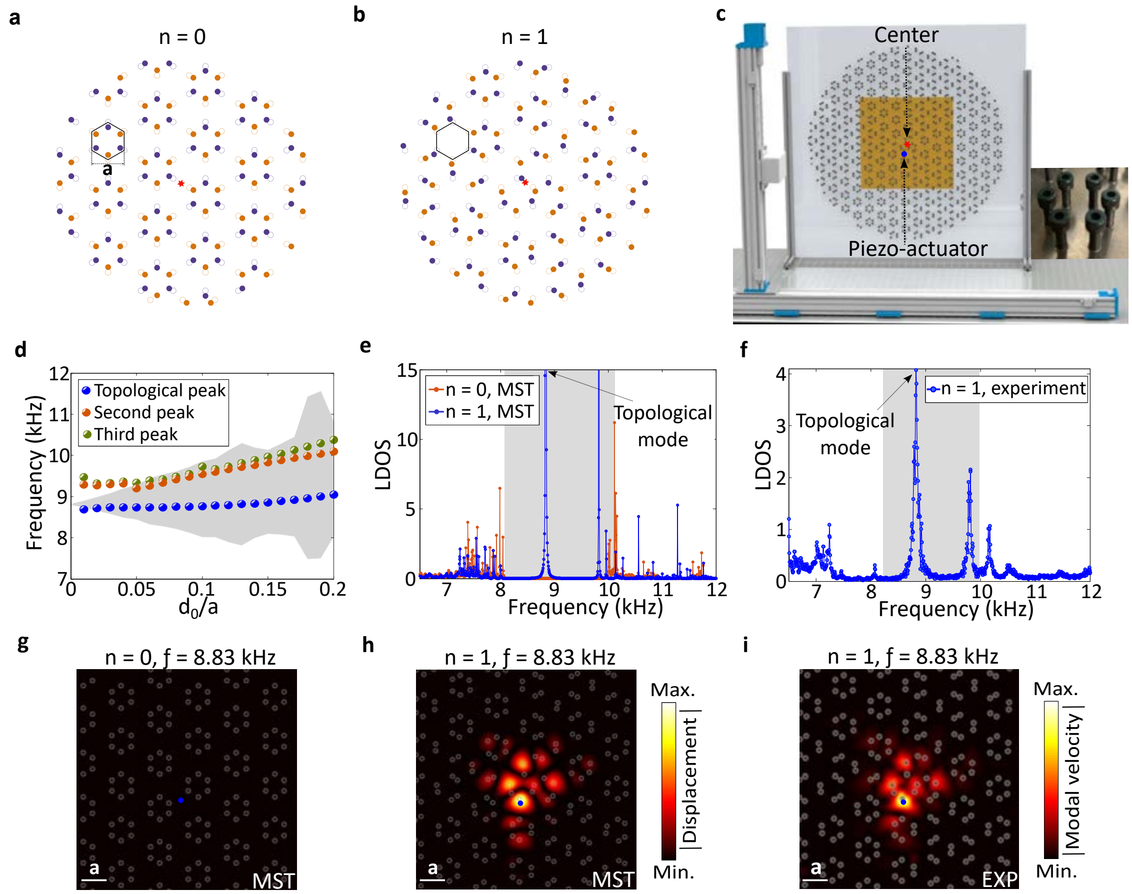

FIG. 2. **System configuration and the vortex bound states**. **a, b**, No-vortex ($n = 0$) and vortex ($n = 1$) patterns, respectively. The hollow circles containing two sub-lattices in golden and purple denote unperturbed ($d_0 = 0$) honeycomb configuration with lattice period a, whereas the filled circles denote the perturbed configuration as per Eq. (2). The red star denotes the origin. **c**, Experimental setup, in which a laser Doppler vibrometer scans the yellow area to measure the out-of-plane response of the $n = 1$ vortex lattice. The pattern contains 1069 bolts mounted on a thin aluminium plate as shown in the inset. The blue dot represents the location where the piezoelectric actuator has been mounted. **d**, MST predictions of the bandgap opening (in grey) and the three localized states that become bound as one increases the perturbation strength d_0/a for $n = 1$. The topological peak converges to the Dirac point as the perturbation is reduced to zero. The other two peaks enter the continuum for small perturbations. From this point on the vortex amplitude is fixed to $d_0/a = 0.15$. **e**, LDOS at the core, predicted by MST for the $n = 0$ and $n = 1$ structures. **f**, Measured LDOS verifying the presence of localized states inside the bandgap. **g**, Spatial profile of the out-of-plane displacements within the bandgap when the $n = 0$ structure is excited at the blue point. **h, i**, Simulated displacements and measured power spectral density for $n = 1$ at their corresponding frequencies.

elastic plate takes the form of a strongly localized vibrational mode of flexural wave motions and out-of-plane bolt vibrations as visualized in Fig. 1.

To confirm this prediction we fabricate the vortex-hosting configuration using the bolted-plate design and performed measurements with a laser Doppler vibrometer (LDV). In Fig. 2c, we show the experimental setup, in which a piezoelectric actuator excites the core of the vortex, and the LDV takes point-by-point measurements of the plate to reconstruct the wave field in the entire scanned area (see Methods). The results are analyzed by comparing them to numerical computations based on the multiple scattering theory (MST) where the bolts are modelled as resonators with an effective out-of-plane stiffness (see Supporting Information for details) [41].

For fixed $n = 1$ we vary the gap opening perturbation d_0, and numerically compute the local density of states (LDOS) (see Methods for more details). In Fig. 2e, we plot the emerging spectral peaks and bandgap region (grey region) as we increase the perturbation d_0 in the vortex. For $d_0 = 0$, we recover the unperturbed honeycomb lattice hosting a double Dirac cone at a Dirac frequency of 8.83 kHz. A nonzero d_0 couples the two valleys, thus gapping the two Dirac cones and lifting their degeneracy, with a gap that increases with d_0. Within this bandgap, several localized states emerge. Figure 2d illustrates that particularly one state always remains bound inside the gap, and converges within our precision to the Dirac frequency as the perturbation d_0 approaches zero. Since a topological state can be eliminated only by closing a bulk bandgap, we claim that the first peak (blue dots in the figure) corresponds to the topological bound state in our system. The other two states are topologically trivial, since they merge with the continuum below a finite d_0, at which point they become delocalized.

In Fig. 2e we plot in blue the $n = 1$ normalized LDOS, computed for fixed $d_0 = 0.15a$, with the topological mode highlighted. To corroborate its topological origin, we also include in red the LDOS results for the zero-winding $n = 0$, $\xi \to 0$ configuration of Fig. 2a, which should not trap topological states. Its LDOS shows a similar bandgap, but with peaks clustering around the edges of the bandgap. We experimentally verify the existence of vortex-localized states by plotting the measured normalized LDOS in Fig. 2f. We detect three localized states at frequencies 8.83 kHz (topological), 9.81 kHz, and 10.17 kHz. We attribute the slight frequency mismatch between MST and experiments to fabrication errors and to the fact that the MST model only captures the out-of-plane motion of the bolts [42].

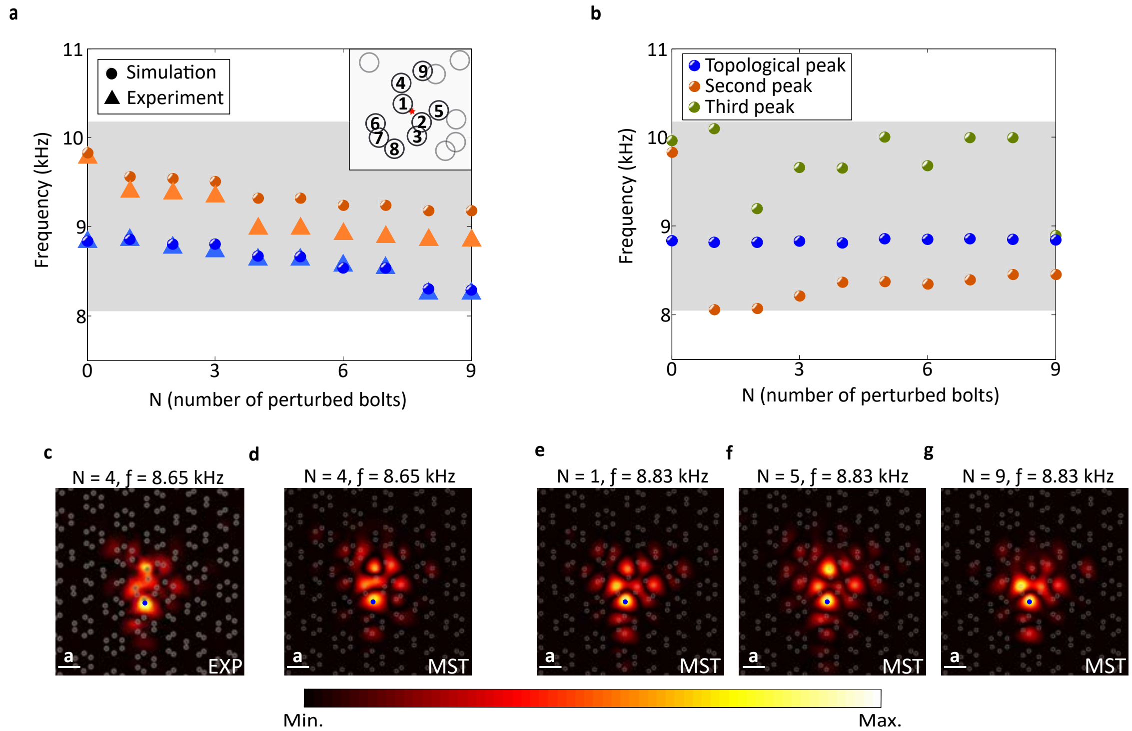

FIG. 3. **Topological robustness with and without particle-hole symmetry.** **a**, Dependency of the in-gap bound state frequencies with an increasing number of mass-loaded bolts. **b**, Bound state frequency evolution under PH-symmetry-preserving perturbations. Note the frequency pinning of the topological mode. Insets show an enlarged view of the vortex core with numbered perturbation sites. **c,d**, Measured and simulated bound state map when $N = 4$ bolts are perturbed through mass-loading. **e–g**, Simulated, mechanical bound states protected by particle-hole symmetry for $N = 1$, $N = 5$, and $N = 9$, respectively.

The computed spatial profile of the displacement field at 8.83 kHz, excited by the point-like actuator shown in Fig. 2c, indicates that the topological mode is concentrated at the $n = 1$ vortex core (Fig. 2h), while the displacement field is hardly visible in the $n = 0$ non-resonant case (Fig. 2g). This prediction is closely matched by the measured mode profile shown in Fig. 2i.

Topological bound states within a given symmetry class are special in that they cannot be removed out of the gap by arbitrary local perturbations that remain in the same symmetry class. Similar to the case of Majoranas in vortices of p-wave superconductors, we expect that our bound state will remain pinned at the Dirac point under any applied perturbation, as long as it preserves the particle-hole (PH) symmetry associated to its topological class. If symmetry-preserving (but otherwise arbitrary) disorder of this form is applied to the sample around the vortex region, the topological bound state will remain entirely robust and fixed at Ω_D. To confirm the topological nature of the 8.83 kHz mode trapped at the vortex, we now study its behavior as local perturbations are added to the core region. We first introduce a small local perturbation by adding a mass by fastening two nuts (with $\sim$41% mass of each bolt) to N bolts sequentially as indicated in insert of Figs. 3a. The mass-loading perturbation does not preserve the PH symmetry of the original symmetry class, and hence the topological bound state is not protected against this type of perturbation. As the number N of loaded bolts is increased, all modes shift, including the topological one, and may even move out of the gap. Before exiting the gap, however, the experimental and numerical field maps of the topological mode remain remarkably insensitive to the perturbation, as can be seen by comparing Figs. 3c,d to Figs. 2h,i. This result highlights the topological mode's exceptional robustness even against symmetry-breaking local mass perturbations. Additional measurements are found in the Supporting Information. Topological protection as enjoyed by MBSs is stronger, however, and implies a pinning of the mode to the Dirac frequency as the symmetry-preserving perturbation grows. To confirm such topological pinning, we designed a special perturbation that preserves PH symmetry by simultaneously changing the bolt stiffness and mass (see Supporting Information). We show numerically that this perturbation, sequentially added to the same set of bolts, shifts the energy of all modes in the gap except for the topological mode, which indeed remains pinned at 8.83 kHz, see Figure 3b. In addition, like in the mass loading experiment, the spatial profile of the non-trivial mode remains essentially insensitive to the local perturbations, see Figs. 3e-g. These observations are a strong confirmation that the mode is topologically confined, as corresponds to a mechanical analogue of a Majorana bound state.

We numerically and experimentally demonstrated that a mechanical analogue of a MBS, where valley plays the role of the particle-hole sector, can exist in artificial structures hosting a non-trivial Kekulé vortex. We specifically showed the effect on the topologically bound mode of local-mass perturbations and PH symmetry-preserving perturbations. In contrast to other trivial bound states in the system, we showed that the topological mode is completely insensitive to PH-symmetric perturbations, which confirms its unique topological character. We foresee that our findings will widen the research of exotic topological phases in bosonic settings and could stimulate robust control and guiding of mechanical energy for signalling and filtering applications.

---

[1] Yang, Z. *et al.* Topological acoustics. *Phys. Rev. Lett.* **114**, 114301 (2015).

[2] He, C. *et al.* Acoustic topological insulator and robust one-way sound transport. *Nat Phys.* **12**, 1124 (2016).

[3] Lu, J. *et al.* Observation of topological valley transport of sound in sonic crystals. *Nat Phys.* **13**, 369–374 (2017).

[4] Zhang, X., Xiao, M., Cheng, Y., Lu, M.-H. & Christensen, J. Topological sound. *Commun. Phys.* **1**, 97 (2018).

[5] Wang, P., Lu, L. & Bertoldi, K. Topological phononic crystals with one-way elastic edge waves. *Phys. Rev. Lett.* **115**, 104302 (2015).

[6] Süsstrunk, R. & Huber, S. D. Observation of phononic helical edge states in a mechanical topological insulator. *Science* **349**, 47–50 (2015).

[7] Chaunsali, R., Chen, C.-W. & Yang, J. Subwavelength and directional control of flexural waves in zone-folding induced topological plates. *Phys. Rev. B* **97**, 054307 (2018).

[8] Miniaci, M., Pal, R. K., Morvan, B. & Ruzzene, M. Experimental observation of topologically protected helical edge modes in patterned elastic plates. *Phys. Rev. X* **8**, 031074 (2018).

[9] Ozawa, T. *et al.* Topological photonics. *Rev. Mod. Phys.* **91**, 015006 (2019).

[10] Kitaev, A. Y. Unpaired majorana fermions in quantum wires. *Phys. Usp.* **44**, 131 (2001).

[11] Fu, L. & Kane, C. L. Superconducting proximity effect and majorana fermions at the surface of a topological insulator. *Phys. Rev. Lett.* **100**, 096407 (2008).

[12] Kekulé, A. Untersuchungen über aromatische verbindungen. *Ann. Chem. Pharm.* **137**, 129 (1866).

[13] Hasan, M. Z. & Kane, C. L. *Colloquium* : Topological insulators. *Rev. Mod. Phys.* **82**, 3045–3067 (2010).

[14] Kane, C. L. & Lubensky, T. C. Topological boundary modes in isostatic lattices. *Nat Phys* **10**, 39–45 (2013).

[15] Nash, L. M. *et al.* Topological mechanics of gyroscopic metamaterials. *Proc Natl Acad Sci* **112**, 14495–14500 (2015).

[16] Pal, R. K. & Ruzzene, M. Edge waves in plates with resonators: an elastic analogue of the

quantum valley hall effect. *New J. Phys.* **19**, 025001 (2017).

[17] Paulose, J., Chen, B. G.-g. & Vitelli, V. Topological modes bound to dislocations in mechanical metamaterials. *Nat Phys* **11**, 153–156 (2015).

[18] Prodan, E., Dobiszewski, K., Kanwal, A., Palmieri, J. & Prodan, C. Dynamical majorana edge modes in a broad class of topological mechanical systems. *Nature Communications* **8**, 14587 (2017).

[19] Iadecola, T., Schuster, T. & Chamon, C. Non-abelian braiding of light. *Phys. Rev. Lett.* **117**, 073901 (2016).

[20] Menssen, A. J., Guan, J., Felce, D., Booth, M. J. & Walmsley, I. A. A photonic majorana bound state. *arXiv* 1901.04439 (2019).

[21] Serra-Garcia, M. *et al.* Observation of a phononic quadrupole topological insulator. *Nature* **555**, 342 (2018).

[22] Noh, J. *et al.* Topological protection of photonic mid-gap defect modes. *Nature Photonics* **408**, 12 (2018).

[23] Zhang, Z., Rosendo López, M., Cheng, Y., Liu, X. & Christensen, J. Non-hermitian sonic second-order topological insulator. *Phys. Rev. Lett.* **122**, 195501 (2019).

[24] Jackiw, R. & Rebbi, C. Solitons with fermion number 1/2. *Phys. Rev. D* **13**, 3398–3409 (1976).

[25] Majorana, E. Teoria simmetrica dell elettrone e del positrone. *Il Nuovo Cimento (1924-1942)* **14**, 171–184 (1937).

[26] Jackiw, R. & Rossi, P. Zero modes of the vortex-fermion system. *Nucl. Phys. B* **190**, 681 – 691 (1981).

[27] Read, N. & Green, D. Paired states of fermions in two dimensions with breaking of parity and time-reversal symmetries and the fractional quantum hall effect. *Physical Review B* **61**, 10267 (2000).

[28] Oreg, Y., Refael, G. & von Oppen, F. Helical liquids and majorana bound states in quantum wires. *Phys. Rev. Lett.* **105**, 177002 (2010). URL `http://link.aps.org/doi/10.1103/PhysRevLett.105.177002`.

[29] Lutchyn, R. M., Sau, J. D. & Das Sarma, S. Majorana fermions and a topological phase transition in semiconductor-superconductor heterostructures. *Phys. Rev. Lett.* **105**, 077001 (2010).

[30] Fu, L. & Kane, C. L. Josephson current and noise at a superconductor/quantum-spin-hall-insulator/superconductor junction. *Phys. Rev. B* **79**, 161408 (2009).

[31] Mourik, V. *et al.* Signatures of majorana fermions in hybrid superconductor-semiconductor nanowire devices. *Science* **336**, 1003–1007 (2012). URL `http://www.sciencemag.org/content/early/2012/04/11/science.1222360.abstract`.

[32] Deng, M. T. *et al.* Majorana bound state in a coupled quantum-dot hybrid-nanowire system. *Science* **354**, 1557–1562 (2016). URL `http://science.sciencemag.org/content/354/6319/1557`.

[33] He, Q. L. *et al.* Chiral majorana fermion modes in a quantum anomalous hall insulator–superconductor structure. *Science* **357**, 294–299 (2017). URL `http://science.sciencemag.org/content/357/6348/294`.

[34] Jäck, B. *et al.* Observation of a majorana zero mode in a topologically protected edge channel. *Science* eaax1444 (2019). URL `http://science.sciencemag.org/content/early/2019/06/12/science.aax1444.abstract`.

[35] Nayak, C., Simon, S., Stern, A., Freedman, M. & Das Sarma, S. Non-abelian anyons and topological quantum computation. *Rev. Mod. Phys.* **80**, 1083–1159 (2008).

[36] Wilczek, F. Majorana returns. *Nat. Phys.* **5**, 614–618 (2009). URL `http://dx.doi.org/10.1038/nphys1380`.

[37] Wilczek, F. Majorana modes materialize. *Nature* **486**, 195–196 (2012). URL `https://doi.org/10.1038/486195a`.

[38] Elliott, S. R. & Franz, M. *Colloquium* : Majorana fermions in nuclear, particle, and solid-state physics. *Rev. Mod. Phys.* **87**, 137–163 (2015).

[39] Ivanov, D. A. Non-abelian statistics of half-quantum vortices in p-wave superconductors. *Phys. Rev. Lett.* **86**, 268–271 (2001).

[40] Nishida, Y., Santos, L. & Chamon, C. Topological superconductors as nonrelativistic limits of jackiw-rossi and jackiw-rebbi models. *Phys. Rev. B* **82**, 144513 (2010).

[41] Torrent, D., Mayou, D. & Sánchez-Dehesa, J. Elastic analog of graphene: Dirac cones and edge states for flexural waves in thin plates. *Phys. Rev. B* **87**, 115143 (2013).

[42] Chaunsali, R., Chen, C.-W. & Yang, J. Experimental demonstration of topological waveguiding in elastic plates with local resonators. *New Journal of Physics* **20**, 113036 (2018).

[43] Shore, J. D., Huang, M., Dorsey, A. T. & Sethna, J. P. Density of states in a vortex core and

the zero-bias tunneling peak. *Phys. Rev. Lett.* **62**, 3089–3092 (1989).

ACKNOWLEDGEMENTS

J. C. acknowledges the support from the European Research Council (ERC) through the Starting Grant No. 714577 PHONOMETA and from the MINECO through a Ramón y Cajal grant (Grant No. RYC-2015-17156). J. Y. gratefully acknowledges the support from the NSF (CAREER1553202 and EFRI-1741685). P. S-J. acknowledges support from MINECO/FEDER through Grant No. FIS2015-65706-P. N.L and J.V.A. acknowledge financial support from MINECO grant FIS2015-64886-C5-5-P. D.T. acknowledges financial support through the "Ramón y Cajal" fellowship under grant number RYC-2016-21188.

COMPETING INTERESTS

The authors declare no competing interests.

METHODS

Sample fabrication

The sample is made of a thin aluminum 6061-T6 plate ($762 \times 762 \times 2$ mm) and M4 black-oxide alloy steel bolts [42]. The lattice size a is 26 mm. First, we machined and threaded 1069 holes on the plate using a CNC milling machine. We ensured that the bolts were firmly and equally fastened by taking advantage of the partially threaded bolts, in which the thread-less part can be used as limiter. We then used an electric screwdriver to tighten the bolts with the same torque. At the same time, we added an instant-bond adhesive (Loctite® 431) on the threads to secure the contact between the bolts and the plate. For the robustness study, we attached two zinc-plated steel nuts (1.4 g in total) at the bottom of each bolt (3.4 g).

Experimental measurements and post-processing

We bonded a piezoelectric ceramic disc actuator (STEMiNC, diameter 10 mm, and thickness 1 mm) with a conductive silver epoxy adhesive just below the center of the plate, at which the topological mode has the maximum out-of-plane displacement. We send a frequency-chirped signal (2–20 kHz in 100 ms) from a function generator to the actuator via a voltage amplifier. We used a laser Doppler vibrometer (Polytec OFV 5000) to detect these vibrations. The device was mounted on a 2-axis linear stage, automated to scan a 2D area on the plate. We conducted point-by-point measurements in a square grid (7.5 $\times$ 7.5 mm) and collected the velocity-time history of 1600 points in total inside the yellow region shown in Fig. 2c. All the measurements were synchronized with respect to the onset of the input voltage signal of the function generator. We performed a fast Fourier transformation (FFT) on these velocity-time histories and obtained the power spectral of density (PSD) to reconstruct a 2D field map at a given frequency. We further calculated the LDOS by summing the squared PSD for all points in the scanning area.

Modelling

The multiple scattering method is employed to solve the plate biharmonic equation coupled to a cluster of harmonic oscillators. We compute the plate displacement field as a superposition of a known harmonic incident wave $\psi_0(\vec{r}, t) = \psi_0(\vec{r})e^{i\omega t}$ and the iterated scattered wave at each resonator (see Supporting Information) [41].

Each resonator is modelled as a point scatterer. The incident wave is taken as a point source. The plate stiffness, width and density together with the harmonic oscillator masses and spring constants are encoded in two dimensionless parameters, Ω_R and γ_R. These two quantities define uniquely the Dirac frequency Ω_D for the undistorted lattice (see Supporting Information for details). In this article we use $\Omega_R = 2.15$ and $\gamma = 10$. The spatial integration of absolute value of the displacement field is proportional to the local density of states (LDOS).